RSC Applied Interfaces

ROYAL SOCIETY OF CHEMISTRY

PERSPECTIVE

View Article Online
View Journal

Cite this: DOI: 10.1039/d6lf00045b

Important but often overlooked issues in heterojunction photocatalysts

Hanggara Sudrajat, *[a] Ari Susanti[b] and Muharani Asnal [c]

When appropriately constructed, heterojunctions in photocatalysts can significantly enhance light absorption, charge separation, surface reaction yields, and photostability, thereby improving overall performance. However, the mechanisms behind the improved performance are often misassigned due to incomplete physicochemical characterization, reliance on indirect evidence, and the widespread use of oversimplified band structure models. This Perspective highlights common diagnostic pitfalls and emphasizes that the actual interfacial energetics after semiconductor contact determine the true charge-transfer pathways. We outline a practical, multi-technique approach combining surface potential mapping, photoexcited carrier dynamics, radical identification, and operando measurements to reliably distinguish heterojunction configurations. We further discuss key considerations for material selection. These guidelines aim to support the mechanism-driven design of heterojunction photocatalysts for improved performance.

Received 16th February 2026,
Accepted 10th April 2026

DOI: 10.1039/d6lf00045b

rsc.li/RSCApplInter

1. Introduction

The development of heterojunction photocatalysts has emerged as an important theme in modern materials chemistry and solar energy conversion. The heterojunction concept, based on creating an interface between at least two semiconductors to enhance charge separation and broaden light absorption,[1–3] has evolved from early type-II configurations to more advanced architectures capable of precisely modulating charge carrier dynamics.

To improve photocatalytic performance, increasing attention has been directed toward heterostructure engineering and interface design as key strategies. For example, composite systems integrating materials such as graphitic carbon nitride (g-C_3N_4) with ferrites promote interfacial charge transfer and structural defect formation, leading to enhanced carrier separation and light utilization.[4,5] g-C_3N_4 is widely recognized as an ideal platform for heterojunction formation owing to its tunable electronic structure, visible-light responsiveness, and strong interfacial compatibility.[6,7] Beyond pollutant degradation, these design strategies also play a crucial role in photocatalysis-driven antimicrobial performance.[8] Enhanced charge separation facilitates the generation of reactive oxygen species (ROS), such as ·OH, $\cdot O_2^-$, and H_2O_2, which induce oxidative stress, membrane damage, and ultimately microbial cell death.

With thousands of reports demonstrating superior activity compared to single-component photocatalysts, the belief that assembling two semiconductors intrinsically improves performance has become deeply embedded in the photocatalysis community. However, the rapid expansion of heterojunction research has also produced substantial conceptual ambiguity. The term "heterojunction" is now applied widely to systems that differ not only in composition and morphology, but also in fundamental charge-transfer behavior and interfacial energetics. Too often, the underlying mechanism is assigned solely from isolated semiconductor band positions, with little attention paid to how those bands shift following contact and Fermi-level equilibration. This basic misconception frequently leads to inaccurate mechanistic claims, most notably, the tendency to classify Z-scheme or S-scheme systems as type-II simply because of nominal band alignment from Mott–Schottky analysis or valence-band X-ray photoelectron spectroscopy (VB-XPS). Such interpretations ignore the important fact that the functional mechanism of a heterojunction is defined not by the intrinsic bands of the isolated semiconductors, but by the reconstructed energy landscape at the interface.

In reality, the heterojunction is an electrostatically reconfigured system, shaped by electron redistribution, local dipole formation, and interfacial band bending.[9] The internal electric field that arises upon contact governs whether electrons and holes separate beneficially or whether reactive carriers are instead forced into lower-potential states that compromise photocatalytic activity. An apparently favorable

[a] Quantum Catalysis Group (Q-cat), Research Center for Quantum Physics, National Research and Innovation Agency (BRIN), South Tangerang 15314, Indonesia. E-mail: hanggara.sudrajat@brin.go.id
[b] Department of Chemical Engineering, State Polytechnic of Malang, Malang 65141, Indonesia
[c] SpectraBridge Research Consulting, Tengku Bey Street C4/8, Pekanbaru 28284, Indonesia

"type-II" band arrangement may actually result in severely weakened redox power, while a Z-scheme or S-scheme mechanism, despite involving selective recombination, can retain strong driving forces for multi-electron reactions such as water splitting or CO_2 reduction. Proper mechanistic assignment therefore requires converging lines of evidence tied directly to reactive charge carriers, rather than overreliance on any single characterization technique.

Compounding this problem is a disproportionate focus on electron-driven reduction chemistry while oxidation pathways remain comparatively underexplored. Oxidative half-reactions are kinetically sluggish and highly sensitive to defect states and surface binding environments. Fundamentally, photogenerated holes are also characterized less frequently than electrons, primarily because holes are less visible spectroscopically.[10] Even when electrons are efficiently extracted to drive reduction, trapped or immobile holes may accumulate, causing interfacial degradation or suppressing turnover. Thus, it is insufficient to demonstrate only quenching of photoluminescence (PL) or increased transient electron lifetimes, true catalytic enhancement requires balanced improvements in both half-reactions, reflected in sustained reaction rates and chemical selectivity.

Another critical yet overlooked aspect of heterojunctions lies in their structural and chemical complexity. The vast majority of reported interfaces are far from idealized atomically abrupt boundaries. Real materials inevitably contain interdiffusion zones, grain boundaries, oxygen vacancies, and disordered surface layers, all of which may redirect or dissipate carriers.[11,12] Under operational conditions, these interfaces are not static. Illumination, reactive gases, and electrochemical environments induce surface reconstruction and dynamic changes in oxidation state, meaning the working interfacial energetics can differ dramatically from the pristine structure typically characterized *ex situ*. Buried interfaces further challenge experimental validation,[13] since many surface-sensitive probes fail to capture where charge separation truly occurs. Advances in operando scanning transmission electron microscopy (STEM), ambient-pressure XPS, ultrafast spectroscopy, and electron holography now allow us to better resolve such evolving interfacial states, although these techniques remain underutilized when deriving mechanistic conclusions.

Similar shortcomings arise in the interpretation of characterization data. Commonly employed measurements such as Mott–Schottky and PL spectroscopy are frequently misused as definitive indicators of band energies or separation efficiency, despite being sensitive to artifacts from surface states and defect-mediated recombination. In contrast, rigorous mechanistic evaluation demands techniques that elucidate the actual fate of reactive charge carriers, including transient absorption spectroscopy (TAS), bias-dependent photocurrent studies, Kelvin probe force microscopy (KPFM), isotopic tracing, and reaction-specific scavenger experiments. In combination with theoretical modeling of interfacial electronic structure, such techniques enable reliable discrimination between competing heterojunction mechanisms grounded in semiconductor physics rather than inference.

Moreover, the way in which heterojunction photocatalysts are evaluated continues to distort progress in the field. Highly favorable reaction conditions such as sacrificial reagents, extreme pH, high catalyst loading, and intense artificial illumination routinely inflate performance metrics while obscuring realistic kinetic limitations. Long-term stability is frequently neglected, despite strong evidence that heterojunction interfaces may degrade *via* ion migration, phase transformation, or irreversible accumulation of inactive surface species.[2,14–16] The field will greatly benefit from standardized reporting practices, meaningful benchmarking, and increased emphasis on earth-abundant compositions, durability, and scalability.

These overlooked issues reveal that heterojunction design must evolve from empirical material pairing toward intentional engineering of interfacial electrostatics. Future advances will rely on strategies that exploit charge-selective contacts, tailored dipoles, defect-modulated carrier pathways, and cooperative catalyst–semiconductor interactions. The integration of theoretical predictions with operando studies will accelerate the establishment of robust design principles that apply across diverse material classes. Heterojunctions should no longer be conceived merely as structural assemblies of two semiconductors, but instead as dynamically tuned electrical landscapes that sustain robust charge flow throughout the complete catalytic reaction. In this Perspective, we discuss the aforementioned issues with the aim of guiding the construction of highly active heterojunction photocatalysts.

Although heterojunction photocatalysts have been widely discussed in previous reviews,[17–24] this Perspective offers a meaningfully different viewpoint. Rather than reiterating classifications of heterojunction architectures or summarizing material systems, we focus on the systematic misassignment of charge-transfer mechanisms and the underlying reasons such misinterpretations persist. The key conceptual contribution of this Perspective is the shift from static band-alignment thinking toward an interface-centric, post-contact energetics framework. We emphasize that the functional behavior of heterojunction photocatalysts is governed by Fermi-level equilibration, band bending, and interfacial electric fields that emerge only after semiconductor contact, which are factors that are overlooked or implicitly assumed in prior reviews. By critically examining how commonly used techniques are misapplied, this work identifies why fundamentally different heterojunction systems are often indistinguishable under conventional diagnostic approaches.

Beyond identifying these limitations, this Perspective proposes a practical, multi-modal diagnostic framework that integrates spectroscopic, electrochemical, and catalytic evidence to enable reliable mechanistic assignment. In doing

so, it moves beyond descriptive reviews by offering actionable criteria and cross-validation strategies that directly connect characterization outputs with physically meaningful charge-transfer pathways. Importantly, the discussion is also expanded beyond mechanism identification to include materials selection, defect effects, and realistic operating conditions, thereby linking interfacial physics with catalytic performance and long-term stability. This holistic approach distinguishes the present Perspective from existing literature, which typically treats mechanism classification, material design, and application considerations in isolation. All in all, the novelty of this contribution lies in establishing a rigorous, mechanism-driven paradigm for heterojunction photocatalysis, aimed at reducing ambiguity and guiding the rational design of next-generation heterojunction photocatalysts.

2. Configuration assignment

When constructing a heterojunction photocatalyst, the first fundamental question is: what heterojunction configuration is formed? This question is far from trivial and requires correct characterization methods together with rigorous interpretation of the resulting data. Despite the rapid growth of heterojunction photocatalysis research, a major conceptual challenge persists: heterojunction types, and consequently charge-transfer mechanisms, are frequently misassigned because conclusions are drawn from incomplete evidence or oversimplified semiconductor band diagrams that fail to represent the actual interfacial physics. As emphasized in recent foundational analyses of semiconductor interfaces,[25,26] the actual behavior of carriers is governed not by the flat-band positions of isolated semiconductors, but by the energetic landscape that emerges only after intimate contact and Fermi-level equilibration. This means that the heterojunction type cannot be correctly deduced from individual band-edge diagrams or UV–vis-based bandgap estimates alone. Instead, determining the true mechanism requires a multi-modal diagnostic strategy that integrates structural, electronic, interfacial, and catalytic observations into a coherent interpretation.

The first step toward accurate heterojunction elucidation is to realize the distinction between intrinsic energy levels of each semiconductor and the effective interfacial band structure that forms after electron redistribution. When two semiconductors are brought into contact, electrons flow from the material with the higher Fermi level to the material with the lower Fermi level.[1] This electron migration continues until equilibrium is achieved, producing interfacial band bending whose magnitude and direction depend on the doping density, defect concentration, surface states, and chemical bonding interactions between the two components. It is this band bending, rather than the isolated conduction band (CB) and valence band (VB) positions/potentials, that determines whether photogenerated carriers will transfer downhill (type-II), selectively recombine (Z-scheme or S-scheme), or remain largely confined within their respective materials.

Because interfacial band bending cannot be directly inferred from optical absorption or Mott–Schottky measurements alone, no single characterization technique is sufficient to assign heterojunction type. For example, PL quenching is often cited as evidence for enhanced charge separation, but such quenching can also arise from increased defect-mediated nonradiative recombination or from the introduction of co-catalysts rather than from genuine interfacial carrier transfer. Similarly, observing improved catalytic activity does not inherently indicate the existence of a type-II or Z-scheme mechanism, as performance enhancements may simply result from increased surface area, improved light absorption, or defect engineering unrelated to charge-transfer pathways.

Accurate elucidation thus requires a convergence of evidence. XPS is crucial for identifying Fermi-level shifts through changes in core-level binding energies upon heterostructure formation.[27] If a semiconductor becomes more electron-rich, its binding energies shift to lower values, whereas electron-depleted components shift to higher values. In a true type-II system, electrons accumulate in the semiconductor whose isolated CB minimum (CBM) lies lower in energy. In an S-scheme or Z-scheme system, however, electrons instead accumulate in the strongly reducing component, regardless of the nominal CB alignment. Such XPS shifts provide direct evidence of the electron-migration direction during Fermi-level equilibration. Holes, on the other hand, are considerably more challenging to probe in terms of their migration and transfer pathways, even though oxidation reactions are often the thermodynamic and kinetic bottlenecks in photocatalysis and therefore require thorough characterization. *In situ* XPS further enables a more accurate characterization of electron transfer in heterojunctions by capturing interfacial electronic changes under realistic operational environments.[28]

Electron paramagnetic resonance (EPR) or also known as electron spin resonance (ESR), offers equally powerful insights. Under illumination, the appearance or intensification of reactive oxygen species ($\cdot O_2^-$, $\cdot OH$) indicates the presence of high-energy electrons or holes, which type-II systems inherently suppress. Thus, observing strong oxidative radicals provides supportive evidence for Z-scheme or S-scheme behavior. Time-resolved PL (TRPL) can further clarify carrier lifetime changes. Increases in carrier lifetime consistent with spatial charge separation support type-II or Z-scheme pathways, while disproportional changes suggest surface defect influences instead.

TAS, Kelvin probe measurements, and scanning KPFM (SKPFM) offer deeper insights into the potential gradients that develop at interfaces.[29–32] TAS reveals the population and lifetimes of excited carriers in specific semiconductor components.[31,33] SKPFM directly maps surface potential distributions, permitting visualization of built-in electric fields characteristic of S-scheme structures, for instance.[30]

Similarly, Kelvin probe measurements performed under light and dark conditions reveal illumination-induced shifts in work function, enabling differentiation between uphill and downhill charge transfer behaviors.[29,34]

Ultraviolet photoelectron spectroscopy (UPS) also plays a crucial role in characterizing heterojunction photocatalysts by providing direct measurements of the VB maximum (VBM) and the work function of each semiconductor component.[35] These parameters allow us to determine the energetic driving force for hole transfer and to assess how the Fermi levels equilibrate upon contact. By tracking changes in band positions before and after heterojunction formation, UPS can reveal interfacial band bending and the direction of charge redistribution, thereby supporting a correct mechanistic assignment.

Ultimately, catalytic data serve as the final confirmation. A heterojunction capable of producing strong oxidizing and reducing radicals simultaneously cannot be type-II, as type-II operation inherently weakens redox potential through staggered band offsets. Conversely, if a system only achieves reasonable activity in the presence of sacrificial agents, this may suggest ineffective recombination control or a mechanism dominated by defect-mediated transport rather than a true heterojunction pathway. The ability to perform multi-electron reactions such as overall water splitting or selective CO_2 reduction with high Faradaic efficiency strongly favors S-scheme or Z-scheme interpretations.

Together, these analytical techniques form a methodological framework for heterojunction elucidation. Only through such an integrative approach, where band-structure analysis, interfacial energetics, carrier lifetimes, surface potential mapping, EPR signatures, and catalytic data converge, can us confidently establish the operative mechanism. By adhering to this rigorous framework, the photocatalysis community can avoid conceptual confusion and advance toward the rational design of heterojunction photocatalysts. In Table 1, we summarize the diagnostic criteria used to assign heterojunction types, highlighting the key distinctions among the relevant mechanistic configurations. In this framework, post-contact band alignment serves as the primary basis for classification, whereas morphological features are treated as secondary factors that modify, but do not define, the underlying charge-transfer mechanism.

The rapid expansion of research in heterojunction photocatalysis has been accompanied by an abundance of mechanistic claims, many of which do not withstand rigorous scrutiny. Type-II heterojunctions are the most frequently reported configuration in photocatalysis,[19,36,37] and thus it is unsurprising that the most prevalent issue is the attribution of type-II mechanisms to systems that do not, in fact, operate through a staggered charge-transfer process. Table 2 outlines common pitfalls in the mechanistic assignment of type-II heterojunction. This misinterpretation stems largely from the misleading simplicity of band-structure diagrams derived from VB-XPS and Mott–Schottky measurements.[38] While valuable, these techniques cannot directly determine charge-transfer direction, interfacial band bending, internal electric-field structure, defect states, or the dynamic fate of carriers under illumination.

The misconception also extends well beyond type-II systems. Improved photocatalytic activity is quite often interpreted as evidence of type-II charge separation, despite the fact that several alternative pathways including Z-scheme, S-scheme, p–n junction behavior, and defect-induced internal fields can similarly promote carrier separation. Z-scheme and S-scheme architectures may outperform type-II systems because they retain strong redox potentials rather than sacrificing them for spatial separation. Such oversights not only result in incorrect mechanistic assignments but also obscure the unique advantages of architectures specifically designed to maximize redox capability.

Misinterpretations are also increasingly prevalent in the rapidly expanding S-scheme and Z-scheme literature. Fig. 1 depicts the differences in charge-transfer pathways between these two configurations. A common oversimplification in S-scheme assignments is the assumption that any n–n or n–p heterojunction exhibiting a potential gradient inherently qualifies as an S-scheme. In reality, an S-scheme requires selective interfacial recombination between the less energetic electrons and holes, which must be substantiated by direct experimental evidence (*e.g.*, TAS or reaction-site mapping). Without such validation, designating an S-scheme mechanism is speculative. Similarly, upward and downward band bending is frequently illustrated qualitatively in schematic band diagrams but seldom verified experimentally, leading to conclusions that rely more on conceptual interpretation than on confirmed interfacial energetics.

Misinterpretations of Z-scheme configurations often arise from the confusion between mediated and direct architectures. Physical interfacial contact is commonly used as the sole justification for assigning a system as a "direct Z-scheme", despite a lack of evidence for the defining charge-transfer characteristics of Z-scheme operation: an efficient interfacial recombination channel that selectively annihilates the low-energy charge carriers. Insufficient evidence of recombination mediators (in indirect systems) or of direct interfacial charge transfer (in all-solid-state Z-schemes) frequently leads to mechanistic claims that contradict the actual charge-flow pathway. Moreover, Z-scheme behavior is often incorrectly inferred solely from the preservation of strong redox activity, an appealing yet inconclusive indicator unless validated by kinetic carrier-tracking measurements.

Indeed, differentiating Z-scheme from S-scheme systems remains particularly challenging because both architectures share the same macroscopic functional signatures, which are improved carrier separation, preserved strong redox activity, and reduced recombination.[39] In both cases, selective recombination of the low-energy carriers occurs, leaving the high-energy electrons and holes spatially separated for redox reactions. The key distinction lies in where and how recombination occurs. In Z-schemes, recombination happens

Table 1 Diagnostic criteria for heterojunction type assignment

Heterojunction class	Expected carrier flow and signature	Band bending/internal field	Key spectroscopic indicators	EPR fingerprints	Photodeposition of co-catalysts, if desired, due to electron localization[a]	Diagnostic notes
Type-II	• Electrons → lower CB; holes → higher VB (downhill transfer)	• Weak, shallow, often symmetric	• Surface photovoltage spectroscopy (SPV): weak field; KPFM: small potential gradient	• Weak $\cdot O_2^-$, weak ·OH due to energy relaxation	• Metal deposition on lower-energy CB semiconductor	• Most often misassigned; strong-redox radicals should be absent
Direct Z-scheme	• Selective recombination at interface; strong electrons/holes retained	• Moderate interfacial bending; requires clean junction	• TAS: fast recombination + long-lived high-energy carriers	• Strong $\cdot O_2^-$ and ·OH	• Photodeposition on high-energy CB semiconductor	• Requires atomically clean interfaces and detectable selective recombination
Mediator Z-scheme	• Carrier recombination *via* redox shuttle	• Field absent; mediator governs direction	• Transient spectra of shuttle; redox-state cycling	• Radical signatures similar to direct Z-scheme	• Deposition follows strong-CB semiconductor	• Mechanism confirmed by observing mediator cycling (I^-/IO_3^-, Fe^{3+}/Fe^{2+})
S-scheme	• Built-in field removes weak carriers; strong ones preserved	• Strongly asymmetric band bending	• SPV/KPFM: steep gradients; UPS: Fermi-level shift	• Strong radicals ($\cdot O_2^-$, ·OH)	• Photodeposition on reduction-side component (strong CB)	• Easier to synthesize than Z-scheme; robust under real conditions
p–n junction	• Depletion-driven separation	• Moderate band bending; doping-dependent	• SPV: clear but moderate signal	• Moderate radical generation	• Electrons accumulate on n-side	• Band bending governed by dopant densities; limited redox strength
Core–shell	• Radial transfer through shell; often type-II-like unless band bending dominates	• Shell thickness determines bending strength	• Electron energy-loss spectroscopy/transmission electron microscopy (EELS/TEM): radial potential shifts; SPV through shell	• Radicals are moderate unless designed as an S-scheme	• Deposition depends on shell/core energetics; often on shell if CB lower	• Shell too thick blocks transfer; too thin causes instability
2D–2D van der Waals (vdW)	• Lateral high-mobility transfer; may operate as Z-scheme, S-scheme, or type-II depending on alignment	• vdW contact → field depends on work-function difference	• TRPL: anisotropic lifetimes; KPFM mapping across plane	• Strong radicals if Z/S-scheme; weak if type-II	• Deposition strongly facet-selective	• Mechanism depends sensitively on stacking angle, exfoliation quality, lattice mismatch
Mixed-dimensional (0D/2D, 1D/2D)	• Multidirectional pathways; mechanism determined by dominant interface	• Localized band bending at dimensional junctions	• TAS: coupled multi-timescale dynamics	• Radical intensity varies; diagnostics must decouple dimensional contributions	• Photodeposition on the component with strongest CB	• Mechanistic assignment must consider quantum-confinement and dimensional coupling effects

[a] Co-catalysts for oxidation reactions may also be deposited by VB holes when they accumulate on specific surface facets that are spatially separated from the electron-rich regions.

Table 2 Common misinterpretations in assigning type-II heterojunction mechanisms

Common misinterpretation	Why the interpretation is incorrect	Mechanistic consequence	Correct approach	Commonly misassigned systems
Assigning type-II from isolated CB/VB positions	• Band positions reflect individual materials, not post-contact interface	• Ignores Fermi-level equilibration and built-in fields	• Combine band alignment with KPFM/SPV and work-function analysis	• S-scheme, Z-scheme, 2D–2D, mixed-dimensional
Using PL quenching as proof of type-II	• PL reduction does not indicate transfer direction	• Misinterprets recombination suppression as downhill transfer	• Use TRPL (lifetimes) and TAS (carrier dynamics)	• S-scheme, direct Z-scheme
Increased photocurrent = type-II	• Photocurrent reflects separation efficiency, not mechanism	• Overestimates cascade transfer role	• Pair with photodeposition to locate electrons	• Oxide/g-C_3N_4 systems
Smaller EIS Nyquist arc = type-II	• EIS shows resistance, not carrier direction	• Confuses mobility with mechanism	• Combine with EPR and SPV	• S-scheme systems
Strong radical signals imply type-II	• Type-II weakens redox power → radicals should be weak	• Leads to unrealistic redox expectations	• Strong radicals indicate S- or Z-scheme; confirm *via* EPR	• Oxide–nitride systems
Higher BET surface area indicates type-II	• Surface area affects kinetics, not mechanism	• Misattributes activity improvement	• Use TAS, KPFM, photodeposition for mechanism	• Porous composites
Strong H_2 evolution = type-II	• Type-II has weaker CB electrons	• Mislabels strong-reduction systems	• Confirm electron location experimentally	• g-C_3N_4/sulfide systems
Using intuitive band diagrams only	• Ignores band bending, dipoles, interface states	• Wrong charge-flow prediction	• Construct diagrams using UPS, KPFM, DFT + experiments	• 2D–2D, mixed-dimensional
Optical absorption shifts indicate mechanism	• Shifts arise from confinement or strain	• Overlooks interfacial energetics	• Combine with TAS and electronic structure analysis	• Core–shell, step-scheme
Improved reaction rate proves type-II	• Performance does not reveal charge pathway	• Misconnects kinetics with mechanism	• Use radical profiling, isotopic tracing	• CO_2 reduction systems
Neglecting co-catalyst effects	• Co-catalysts alter charge distribution	• Distorts intrinsic mechanism	• Map charge localization before/after loading	• Pt-, Ni-, Co-based systems
Treating mixed-dimensional systems as type-II	• Dimensional interfaces often create local fields	• Oversimplifies complex interfaces	• Use directional SPV and facet-selective tests	• 0D/2D, 1D/2D
Assuming step-scheme ≈ type-II	• Step-schemes retain partial redox strength	• Loss of mechanistic accuracy	• Identify *via* multi-step TAS signatures	• Ternary/quaternary systems
Using DFT alone	• Often ignores defects, solvent, illumination	• Idealized, unrealistic predictions	• Combine with operando experiments	• Most systems, especially 2D
Ignoring defect-induced fields	• Defects can mimic S-scheme behavior	• Mislabels defect-driven systems	• Use EPR, XPS, deep-level transient spectroscopy (DLTS)	• g-C_3N_4-based
Dye decolorization = degradation	• Color loss ≠ mineralization	• Overestimates activity	• Use total organic carbon (TOC)/chemical oxygen demand (COD) + product analysis	• Dye-based studies
Pollutant removal = complete degradation	• Intermediates may remain toxic	• False environmental relevance	• Perform intermediate tracking + toxicity assessment	• Environmental photocatalysis
Observed activity = intrinsic photocatalysis	• May arise from artifacts (sensitization, pH, heat)	• False mechanism attribution	• Perform control experiments (dark/light blanks, adsorption, self-decomposition of substrate), wavelength-dependent tests, temperature monitoring, and pH tracking	• Poorly controlled studies

at the physical interface (or mediator in indirect systems), whereas S-schemes rely on built-in electric fields and asymmetric band bending that force recombination specifically at the heterojunction interface. Because these dynamic processes cannot be inferred from static band diagrams, accurate classification requires direct evidence of recombination location, carrier movement direction, and interfacial potential gradients, typically obtained through advanced operando spectroscopies or reaction-site mapping. Table 3 summarizes criteria for distinguishing Z-scheme from S-scheme heterojunction configurations.

Other widely misinterpreted indicators, such as PL quenching, enhanced photocurrent, reduced charge-transfer resistance, or increased radical formation, merely reflect improved charge dynamics. They cannot distinguish whether electrons or holes migrate across the interface, nor whether

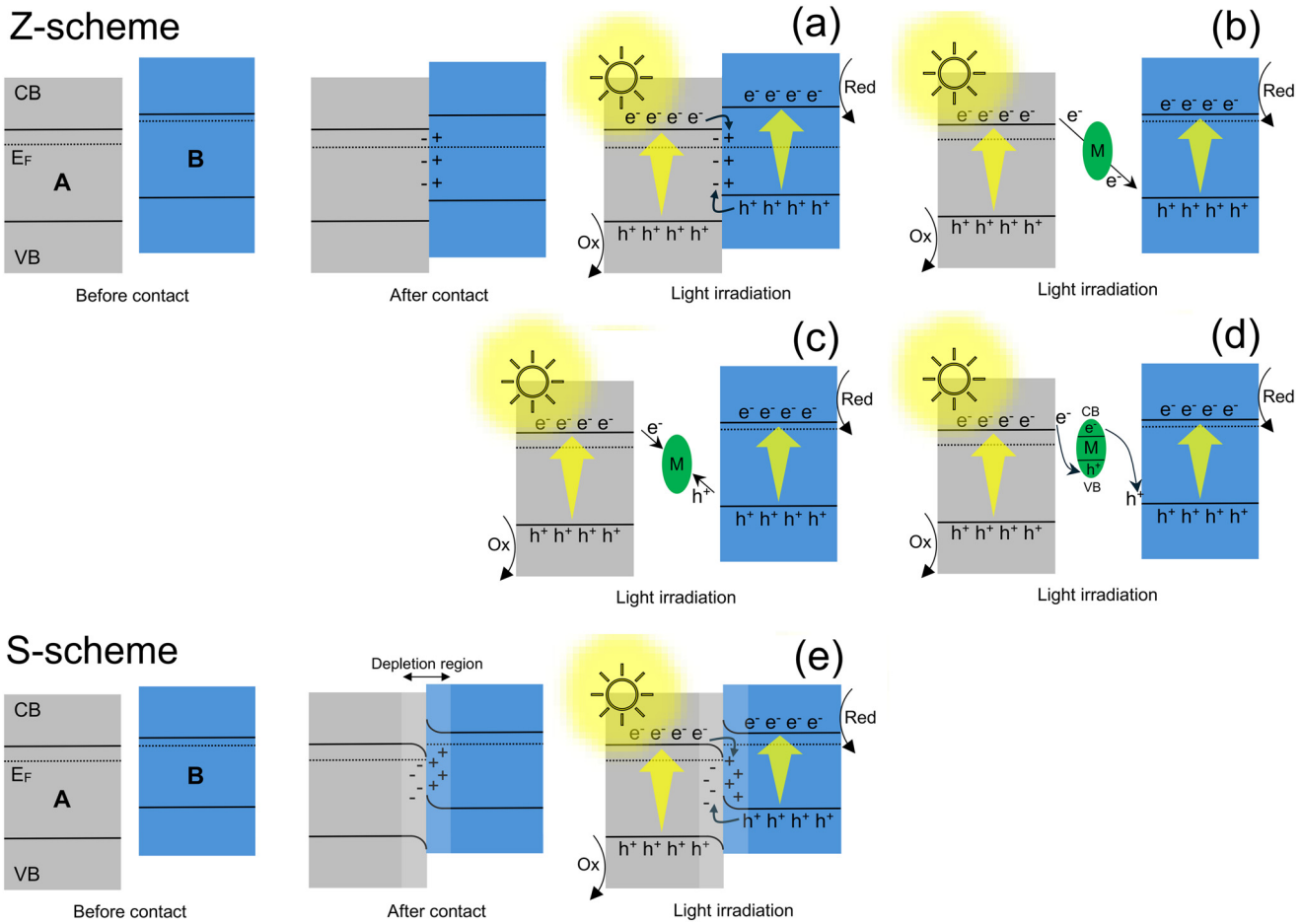

Fig. 1 Band configurations of (a) a direct Z-scheme, (b–d) mediator-assisted Z-schemes, and (e) an S-scheme heterojunction formed between semiconducting materials A and B. M denotes the mediator in mediator-assisted Z-schemes. Mediators are charge-transfer components that shuttle electrons between the two semiconductors to sustain the Z-scheme pathway. They can be redox mediators in solution (*e.g.*, I^-/IO_3^-, Fe^{3+}/Fe^{2+}), solid electron mediators such as noble metals (*e.g.*, Au, Ag, Pt) or carbonaceous conductors (*e.g.*, reduced graphene oxide (rGO), carbon nanotubes (CNTs)), or semiconductor mediators that form stepwise band alignments (*e.g.*, WO_3, TiO_2).

Table 3 Diagnostic criteria for distinguishing Z-scheme and S-scheme heterojunctions

Diagnostic criterion	Direct Z-scheme (all-solid)[a]	S-scheme[b]	Significance
Primary driving force of charge transfer	• Interfacial recombination channel	• Built-in electric field at depletion region	• Reveals fundamental mechanism
Location of selective recombination	• At the physical interface (or mediator in indirect systems)	• Within the space-charge region at the junction	• Defines pathway of low-energy carriers
Band bending requirement	• Not essential (may operate without strong bending)	• Essential, asymmetric up/down bending required	• Confirms field-driven separation
Evidence of recombination mediator	• Required in mediated Z-schemes; absent in direct	• Absent by definition	• Prevents mislabeling mediated systems
Carrier migration direction	• Electrons: CB(A) → interface → recombine with h^+(B)	• Weak e^- in A and weak h^+ in B recombine at junction; strong carriers retained	• Differentiates spatial destination of carriers
Redox strength retention	• Yes, hallmark feature	• Yes, hallmark feature	• Not sufficient alone for assignment
Minimum validation tools	• Selective quenching, ESR/EPR, transient absorption, AP-XPS	• KPFM/SKPM mapping, *in situ* UPS shifts, TAS	• Macroscopic metrics alone insufficient

[a] If selective interfacial recombination or mediator involvement is not shown, Z-scheme remains unverified. [b] If interfacial band bending and direction of carrier drift are not experimentally demonstrated, S-scheme cannot be confirmed.

they recombine selectively as predicted in S-scheme and Z-scheme systems. Static band positions alone are similarly insufficient, because photocarrier accumulation and defect-mediated processes can fundamentally reshape interfacial energetics *in operando*. Collectively, these misconceptions underscore the urgent need for a rigorous, evidence-based framework for heterojunction mechanism identification. Misassignment directly affects whether a photocatalyst retains the redox strength necessary for multi-electron transformations and whether its charge-transfer pathway can support long-term structural and chemical stability. Establishing reliable mechanistic validation is hence essential to accelerate the advancement of heterojunction photocatalysts from promising laboratory demonstrations to robust platforms for solar-driven chemical conversion at scale.

We further provide a schematic to summarize the main concept for mechanism identification. As shown in Fig. 2, a stepwise framework is illustrated for identification of heterojunction charge-transfer mechanisms. The workflow emphasizes that initial band alignment analysis is insufficient and must be complemented by interfacial energetics, carrier dynamics, and reactive species identification. Only through convergence of multi-technique evidence can type-II, Z-scheme, and S-scheme mechanisms be distinguished with confidence. For this purpose, greater weight therefore should be assigned to direct, mechanism-resolving techniques such as EPR, UPS/XPS, KPFM/SPV, and time-resolved spectroscopies, while commonly used indicators such as PL intensity, EIS, and photocurrent responses need to be treated as supportive but non-definitive evidence. The hierarchy of evidence for mechanistic identification in heterojunction photocatalysts is summarized in Table 4.

Moreover, it should be underlined that enhanced photocatalytic performance typically arises from the coupled effects of multiple factors, including surface area and porosity, light harvesting efficiency, charge separation dynamics, and mass transport. Attribution of performance improvements to a single parameter can therefore be misleading. To address this issue, we propose a quantitative framework in which key descriptors such as specific surface area, optical absorption characteristics, charge carrier lifetime, and diffusion-related parameters are treated as interdependent variables (Table 5). Systematic evaluation of these contributions can be achieved through correlation analysis and design-of-experiments (DoE) approaches, involving controlled variation of individual parameters and multivariate analysis. Such an approach enables separation of competing effects and promotes a more rigorous, data-driven understanding of structure–property–performance relationships in heterojunction photocatalysts.

We subsequently highlight representative examples demonstrating the use of the aforementioned measurement techniques to distinguish heterojunction configurations. Using *in situ* irradiated XPS, Guo and co-workers probed charge transfer in Zn–CeO_2/g-C_3N_4.[40] Prior to illumination, the C 1s peak of g-C_3N_4 shifted to lower binding energy, indicating electron transfer from Zn–CeO_2 to g-C_3N_4. Under irradiation, it shifted oppositely, evidencing reversed electron flow. Consistent shifts in Ce 3d peaks corroborated this behavior, confirming an S-scheme mechanism with bidirectional charge transfer. Similarly, Shao and co-workers employed *in situ* XPS on TiO_2/Ti_3C_2.[28] Under UV irradiation, Ti–C shifted negatively while Ti–O shifted positively, indicating electron transfer from TiO_2 to Ti_3C_2 driven by the built-in electric field, characteristic of an S-scheme heterojunction. Ding and co-workers furthermore used SPV to study CdS/Ni–Co (CP) and CdS/NiS (CN) heterojunction photocatalysts.[41] The electron filling lifetimes of the CdS bleaching signal (500 nm) followed CN < CdS < CP, indicating electron transfer from NiS to CdS in CN and from CdS to Ni–Co in CP. Accordingly, CP exhibits type-I transfer, whereas CN shows type-II behavior. Here a type-I heterojunction is defined by a band alignment in which the CBM of semiconductor 1 (SC-1) lies above that of semiconductor 2 (SC-2), while the VBM of SC-1 lies below that of SC-2. Meanwhile, Huang and co-workers applied fs-TAS to a BiOBr/NiFe–LDH (BNF) system.[42] The BiOBr signal appeared at ~0.2 ps, followed by transfer to NiFe–LDH within 0.5–1 ps, confirming electron migration from BiOBr to NiFe–LDH and a Z-scheme mechanism. Meanwhile, Bi and co-workers reported near-infrared-driven H_2O_2 synthesis using a SnS_2/COF heterojunction and employed KPFM to probe charge-transfer behavior.[43] Under illumination (420 nm), the surface potential of TaTp (COF) decreased by 18 mV, whereas SnS_2 increased by 14 mV, consistent with an S-scheme mechanism. The 10% SnS_2/TaTp composite exhibited a larger potential change (23 mV) than the individual components, indicating formation of a strong internal electric field (IEF) at the interface. The calculated IEF strength increased from 2.16 (TaTp) to 4.63 (composite), promoting charge separation and transfer and thereby enhancing photocatalytic performance. Zhong and co-workers investigated a 3D/2D $InVO_4$/g-C_3N_4 heterojunction with N defects for CO_2 reduction using *in situ* KPFM.[44] A 44.3 mV potential difference in the dark indicates a built-in electric field from g-C_3N_4 to $InVO_4$. Under illumination, g-C_3N_4 shows decreased surface potential, while $InVO_4$ exhibits the opposite trend, particularly at the interface. Combined with band alignment analysis, these results confirm an S-scheme charge-transfer mechanism. Likewise, Yu and colleagues investigated a zinc porphyrin/g-C_3N_4 photocatalyst for H_2O_2 production using *in situ* KPFM.[45] The surface potentials of g-C_3N_4 and zinc porphyrin increased from 101 to 189 mV and from 402 to 443 mV under illumination, respectively, with a more pronounced shift for g-C_3N_4. This indicates electron transfer from g-C_3N_4 to zinc porphyrin, confirming an S-scheme mechanism when combined with band alignment analysis.

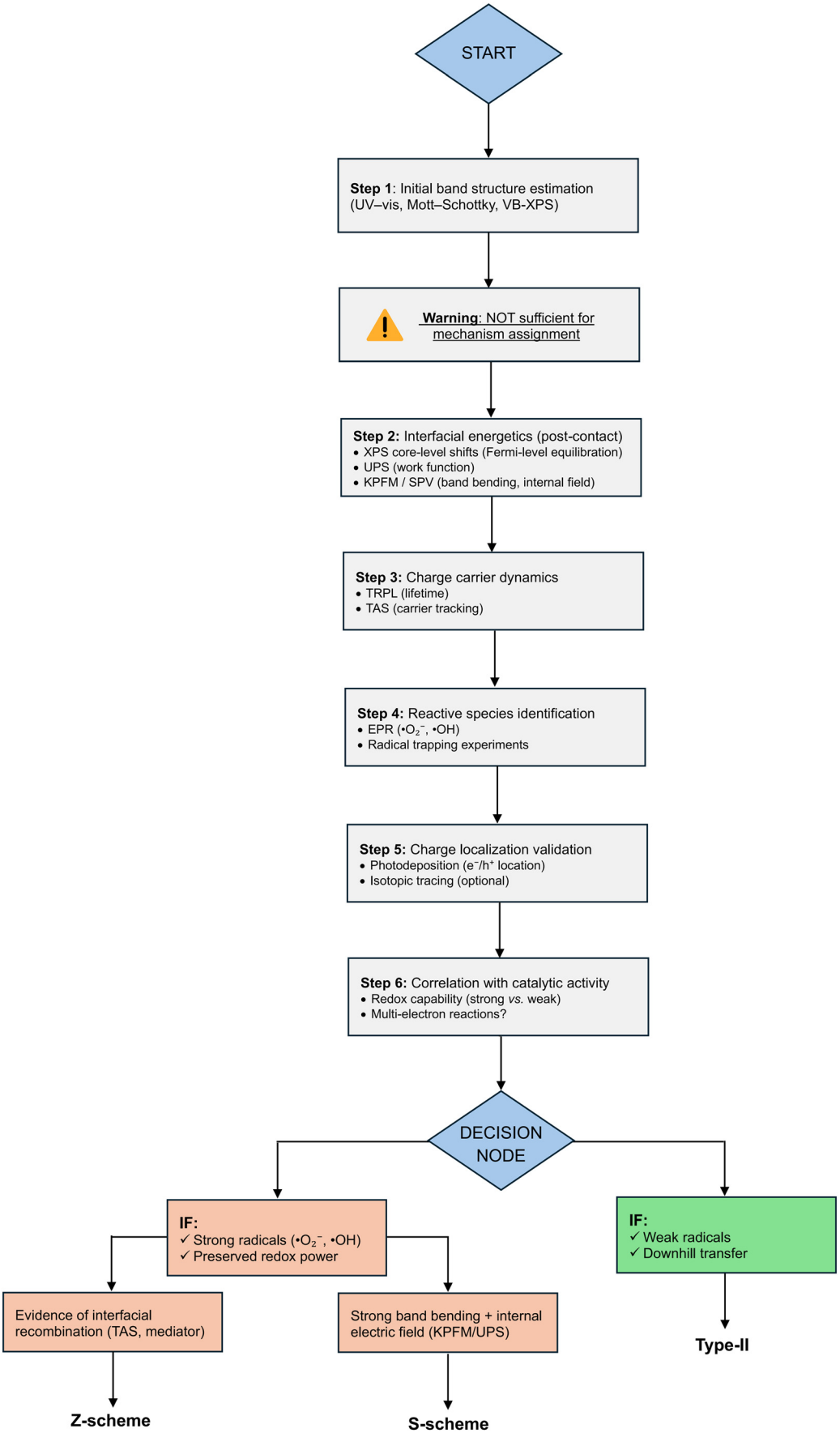

Fig. 2 Framework for identification of heterojunction charge-transfer mechanisms.

Table 4 Hierarchy of evidence for mechanistic identification in heterojunction photocatalysts

Evidence type	Technique	What it directly probes	Strength level	Key limitation	Recommended use
Direct evidence	• EPR (ESR)	• Reactive radicals ($\cdot O_2^-$, $^1O_2$, $\cdot OH$)	• High	• Requires careful interpretation of signals	• Confirm redox pathways
	• UPS/XPS	• Work function, band alignment, Fermi-level shifts	• High	• Surface-sensitive	• Determine interfacial energetics
	• KPFM/SPV	• Band bending, internal electric field	• High	• Requires controlled conditions	• Identify charge-transfer direction
	• TAS/TRPL	• Carrier lifetime and dynamics	• High	• Complex data analysis	• Track recombination pathways
	• Photodeposition	• Spatial charge localization (e^-/h^+)	• High	• Indirect spatial inference	• Validate charge separation sites
	• Isotopic labeling	• Reaction pathway tracing	• High	• Experimental complexity	• Confirm reaction mechanism
	• LC-MS/GC-MS	• Reaction intermediates/products	• High	• Requires careful assignment	• Support pathway validation
	• ICP analysis	• Catalyst stability, leaching	• Moderate–high	• Not directly mechanistic	• Validate catalyst integrity
Indirect proxies/supportive but non-definitive evidence	• Mott–Schottky plots	• Flat band potential	• Moderate	• Ignores interface effects	• Use with UPS/XPS
	• PL intensity (steady-state)	• Recombination tendency	• Low–moderate	• Cannot determine direction of transfer	• Use with TRPL/TAS
	• EIS (Nyquist plot)	• Charge transfer resistance	• Low–moderate	• Not mechanism-specific	• Support transport analysis
	• Photocurrent response	• Charge separation efficiency	• Low–moderate	• No spatial/mechanistic information	• Combine with EPR
	• Band alignment (isolated materials)	• Theoretical charge transfer	• Low	• Not valid post-contact	• Avoid standalone use

Note: techniques classified as "direct evidence" provide mechanism-relevant insights when properly interpreted, whereas indirect methods should not be used in isolation for mechanism assignment and must be corroborated by multiple complementary techniques.

Table 5 Descriptor-based framework for decoupling photocatalytic performance contributions

Descriptor category	Key parameter	Measurement technique	Role in performance	Common confounding effect
Surface properties	• BET surface area, porosity	• N_2 adsorption (BET)	• Active site availability	• Often mistaken for charge separation effect
Light harvesting	• Absorption edge, intensity	• UV–vis DRS	• Photon utilization	• Overlaps with catalyst color/dye sensitization
Charge dynamics	• Carrier lifetime, recombination rate	• TRPL, TAS	• Charge separation efficiency	• Misinterpreted from PL alone
Interfacial energetics	• Band bending, work function	• UPS, KPFM	• Charge-transfer direction	• Ignored in simple band alignment
Mass transport	• Diffusion rate, adsorption kinetics	• Kinetic modeling	• Reactant/product transport	• Hidden in apparent rate constants
Catalytic activity	• Reaction rate, quantum efficiency	• Photocatalytic testing	• Overall performance	• Convolution of all above factors

3. Materials selection

The next fundamental issue is the rational selection of semiconducting materials for constructing heterojunction photocatalysts. Although interfacial charge-transfer mechanisms are central to heterojunction design, the choice of semiconductor components ultimately dictates whether a system can deliver the required photocatalytic performance. Solar-driven transformations such as water splitting, CO_2 reduction, O_2 reduction, and N_2 fixation are intrinsically demanding, necessitating multielectron transfer, strong redox capability, and excellent structural and chemical stability under continuous photoexcitation. Accordingly, careful evaluation of the intrinsic physicochemical properties of candidate semiconductors is essential prior to pairing them into heterojunction architectures. The targeted reaction

pathway should also be considered. Endergonic processes like overall water splitting require highly oxidative VBs and strongly reductive CBs, whereas selective organic conversions typically operate under milder conditions,[46] and thus benefit from more moderate redox potentials. Given this fact, the redox requirements of the desired reaction should be thoroughly assessed before establishing a suitable heterojunction design.

Another concern is photochemical stability. Semiconducting materials often considered as highly active photocatalysts in controlled laboratory environments, including CdS, ZnSe, and Bi_2S_3, may undergo photocorrosion or self-oxidation when exposed to strong oxidative or reductive potentials. In contrast, oxide semiconductors such as TiO_2, WO_3, and Fe_2O_3 exhibit good stability but provide insufficient CB reduction capability. These mismatches highlight the need for rational heterojunction designs that couple strongly reducing semiconductors with oxidation-resistant counterparts to sustain catalytic turnover while preventing structural degradation. Visible-light absorbing sulfides and selenides provide complementary band energies but require protection from photocorrosion, encouraging the use of strategies such as core–shell encapsulation, surface passivation, or partial oxidation to form protective metal oxide layers. Similarly, transition metal dichalcogenides such as MoS_2 and WS_2 offer rich catalytic edge chemistry,[47,48] yet long-term dispersion typically relies on introducing anchoring sites that prevent nanosheet restacking and delamination.

Charge-carrier transport is another important aspect to consider. Photocatalysts with limited carrier mobility can benefit from integration into S-scheme architectures, which generate strong built-in electric fields that facilitate directional charge separation. Incorporating conductive scaffolds such as graphene frameworks, carbon nanotubes, or 3D carbon aerogels can create extrinsic pathways for rapid charge extraction, lowering recombination losses and enabling more efficient utilization of absorbed photons.

Equally important is interfacial compatibility, particularly in direct Z-scheme and S-scheme systems. Interfaces characterized by lattice mismatch, weak adhesion, or defect-induced trapping sites inevitably promote charge recombination, even when the band alignment is favorable. Therefore, material pairings that naturally form chemically robust and electronically complementary interfaces should be prioritized.

Moreover, band alignment should be assessed in electrochemical terms rather than solely from intrinsic CB and VB edges. The operative driving forces in photocatalysis are the redox potentials at the semiconductor–solution interface, which are strongly affected by surface states, defects, Fermi-level pinning, and photocharging. Consequently, mechanistic assignments should not rely exclusively on Mott–Schottky or VB-XPS measurements. Instead, they should be validated through complementary techniques such as TAS, interfacial redox probing, and operando characterization to establish the actual direction of charge transfer. Nevertheless, as an initial guideline, the CB and VB potentials of the constituent semiconductors can be used to roughly estimate a suitable band alignment for the desired charge-transfer pathway and the targeted reaction. Fig. 3 highlights typical semiconductor options for designing heterojunction photocatalysts. Semiconducting materials with highly negative CB positions are better suited for reduction reactions, whereas those with highly positive VB positions are favorable for oxidation. For example, TaON offers band edges insufficient for either strong reduction or strong oxidation, limiting its applicability for such reactions, although it may be still functional in other photocatalytic contexts such as visible-light sensitization. The selection of semiconducting materials determines the resulting heterojunction configuration, its associated

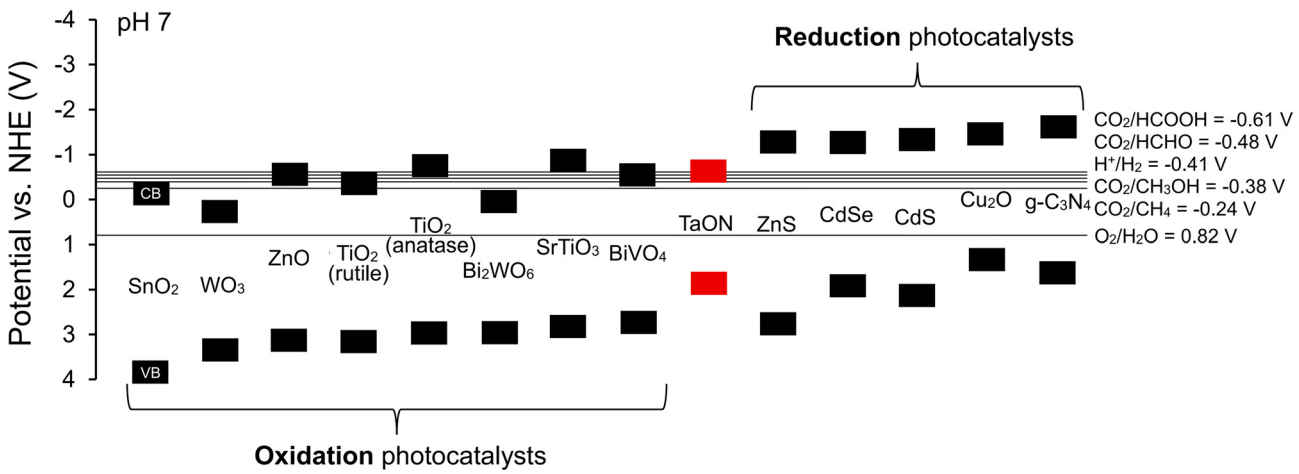

Fig. 3 Typical semiconducting materials to construct heterojunction photocatalysts. For successful photocatalytic operation, the CB and VB edge positions should be appropriately aligned with the redox potentials of the target reactions.

Table 6 Mechanistic and materials comparison of heterojunction architectures

Heterojunction class	Preservation of redox strength	Interface requirements	Material compatibility	Stability and failure modes	Overall mechanistic strengths	Key limitations
Type-II	• No, redox energy is lost due to relaxation	• Moderate; does not require perfect contact	• Works with many oxide/sulfide combinations	• Photocorrosion on reductive component; redox weakening; interface traps	• Simple to synthesize; reliable charge separation in short-term tests	• Not suitable for strong-redox reactions; poor outdoor performance
Direct Z-scheme	• Yes, strong electrons and strong holes retained	• Requires clean, intimate interfaces	• Works with oxides, nitrides, some chalcogenides	• Sensitive to interfacial contamination; delamination possible	• Excellent strong-redox capability; ideal for water splitting	• Interface precision difficult to scale; stability dependent on morphology
Mediator Z-scheme	• Yes	• Low interface precision; solution-phase mediator required	• Wide material flexibility	• Mediator decomposition; back reactions; leaching	• Easy to confirm mechanistically; high redox retention	• Poor long-term stability; impractical industrially
S-scheme	• Yes, preserved and robust	• Requires proper donor/acceptor density; moderate interface quality	• Oxides, nitrides, stable sulfides, carbons	• Very stable; resistant to variable illumination	• Highly robust redox power + stable architecture	• Defect engineering required; too many defects flatten band bending
p–n junction	• Partially	• Requires reliable p- and n-type components	• Narrow range of stable p-type photocatalysts	• p-type photocorrosion common; weak redox preservation	• Simple to fabricate; stable for specific reactions	• Limited VB/CB flexibility; insufficient for fuel generation
Core–shell	• Partially	• Requires precision in shell thickness and contact	• Broad; depends on shell stability	• Shell dissolution; mismatched lattice strain	• Good protection for sensitive cores; scalable	• Overly thick shells block transfer; thin shells degrade
2D–2D van der Waals	• Yes, if Z or S scheme-like	• Requires exfoliation; vdW contact	• TMDs, g-C_3N_4, oxides	• Delamination; stacking misalignment	• High mobility, strong coupling	• Difficult to scale; fragile layer
Mixed-dimensional (0D/2D, 1D/2D)	• Variable	• Moderate	• Many combinations	• Aggregation; mechanical fragility	• Enhanced surface area	• Poor macro-scale stability

charge-transfer pathway, and ultimately the photocatalytic performance. Table 6 compares the mechanistic characteristics and material considerations of different heterojunction architectures.

We should also be aware that constructing heterojunction photocatalysts from earth-abundant materials is important for enabling the widespread deployment of solar-driven chemical conversion technologies and hence needs to be focused. Many high-performing photocatalysts rely on noble metals or scarce elements, whose limited availability, high cost, and environmentally intensive extraction processes present large barriers to scale-up. In contrast, earth-abundant semiconductors offer a more sustainable supply chain while maintaining the potential for strong redox activity, chemical robustness, and tunable band structures when integrated into heterojunction architectures. Earth-abundant compositions improve lifecycle sustainability by minimizing resource depletion and lowering overall environmental footprint. Therefore, prioritizing materials that are both high-performing and geochemically plentiful is a prerequisite for translating heterojunction photocatalysis from laboratory demonstrations to practically viable solar-fuel and environmental remediation technologies. We show materials screening matrix for earth-abundant heterojunctions in Table 7.

Overall, designing active heterojunction photocatalysts requires far more than simply pairing two semiconductors. A holistic screening framework must account for thermodynamic stability, charge mobility, band energetics, interfacial chemical compatibility, surface redox durability, production cost, and even material abundance. Incorporating these considerations enables the transition from empirical semiconductor pairing toward predictive, mechanism-guided selection of components capable of delivering robust and efficient photocatalytic performance.

4. Performance evaluation

One may observe that the current literature quite often shows inconsistent and poorly controlled evaluations of heterojunction photocatalyst performance. To address this issue, we propose an integrated framework that establishes minimum requirements and best practices for the rigorous assessment of heterojunction photocatalysts. As summarized in Table 8, it distinguishes mandatory criteria from recommended practices to ensure reproducible, mechanism-consistent evaluation. Reliance on a single technique or performance metric is insufficient for reliable mechanistic conclusions.

To further strengthen mechanistic rigor and avoid internal inconsistencies, we introduce a thermodynamic–kinetic consistency scheme that integrates band energetics, redox feasibility, ROS evidence, and identified reaction

Table 7 Materials screening matrix for earth-abundant heterojunctions

Functional role	Representative materials	Key advantages	Main limitations	Typical heterojunction pairings
Strong oxidative component (high VB)	• TiO_2, WO_3, $BiVO_4$, Fe_2O_3, SnO_2, Nb_2O_5, ZnO	• Strong oxidation potential, high stability	• Limited reduction ability; ZnO unstable in acid	• TiO_2/g-C_3N_4, WO_3/$ZnIn_2S_4$, $BiVO_4$/MoS_2
Strong reductive component (high CB)	• g-C_3N_4, $ZnIn_2S_4$, ZnS, Cu_2O, MoS_2, WS_2, SnS_2	• Strong reduction capability, tunable bands	• Photocorrosion (sulfides), Cu_2O instability	• g-C_3N_4/WO_3, $ZnIn_2S_4$/TiO_2, MoS_2/$BiVO_4$
Visible-light absorbers (moderate redox)	• Bi_2WO_6, $InVO_4$, $LaFeO_3$, $CuFeO_2$, $FeWO_4$	• Good light absorption, multi-electron reactions	• Moderate stability, limited redox strength	• Bi_2WO_6/g-C_3N_4, $LaFeO_3$/MoS_2
2D layered semiconductors	• g-C_3N_4, MoS_2, WS_2, SnS_2, BiOCl, BiOBr	• High surface area, strong interfacial coupling	• Oxidation (MXenes), air instability (BP)	• g-C_3N_4/MoS_2, BiOCl/$BiVO_4$
Conductive carbon scaffolds	• Graphene, rGO, CNTs, carbon nanosheets	• High conductivity, scalable, inert	• Requires defect control	• TiO_2/rGO, Fe_2O_3/CNT
Mesoporous/high-area supports	• Mesoporous carbon, silica, alumina, hollow carbons	High surface area, good dispersion	• Inert supports may need functionalization	• Z-scheme systems on porous TiO_2/carbon
Earth-abundant HER co-catalysts	• Ni_2P, CoP, Mo_2C, Ni–Mo, Co_3O_4	• Replace noble metals, strong HER activity	• Oxidation (phosphides), synthesis complexity	• g-C_3N_4/Ni_2P, TiO_2/Mo_2C
OER co-catalysts	• Co_3O_4, NiFe-LDH, CoFe-LDH, MnOx	• High OER activity, stable in alkaline media	• Instability in acidic environments	• $BiVO_4$/NiFe-LDH, WO_3/Co_3O_4
Protective/passivation layers	• Al_2O_3, TiO_2, SiO_2, carbon shells	• Improve stability, suppress corrosion	• Must be ultrathin for charge transfer	• $ZnIn_2S_4$@TiO_2, Cu_2O@Al_2O_3
Interface modifiers (field enhancers)	• rGO, MXenes, defect-rich oxides	• Enhance charge transfer, tune work function	• Requires precise defect control	• rGO/TiO_2, defective WO_3/g-C_3N_4
Solid-state charge mediators	• CNTs, graphene, Fe_3O_4, Cu	• Enable directional electron transport	• Risk of short-circuiting	• TiO_2/graphene/g-C_3N_4
Photostable oxide backbones	• TiO_2, ZrO_2, SnO_2, Al_2O_3	• Excellent chemical stability	• Weak light absorption	• g-C_3N_4@TiO_2, $ZnIn_2S_4$@ZrO_2
CO_2 reduction catalysts	• Cu_2O, Fe_2O_3, CeO_2, ZnO	• Tunable selectivity, earth-abundant	• Cu-based instability	• TiO_2/Cu_2O, CeO_2/g-C_3N_4
Industrially robust catalysts	• TiO_2, WO_3, Fe_2O_3, SnO_2, NiO	• Stable under harsh pH/thermal conditions	• Limited redox flexibility	• WO_3/NiO, TiO_2/Fe_2O_3
Macrostructured supports	• Carbon foam, metal foam, ceramics	• Scalable, good mass transport	• Corrosion, need coating	• TiO_2/Fe foam, g-C_3N_4/carbon foam
Biomass-derived supports	• Biochar, lignin carbon, chitosan carbon	• Low cost, sustainable	• Purity and consistency issues	• Biochar/g-C_3N_4, lignin/MoS_2
Non-toxic visible absorbers	• $CuFeO_2$, $ZnFe_2O_4$, Fe_2O_3, WO_3	• Environmentally benign	• Stability limitations (Cu-based)	• $ZnFe_2O_4$/g-C_3N_4, $CuFeO_2$/TiO_2
High work-function semiconductors	• WO_3, Bi_2O_3, MoO_3, Fe_2O_3	• Promote strong built-in fields	Photoinstability (*e.g.*, MoO_3)	• WO_3/g-C_3N_4, MoO_3/MoS_2

intermediates into a unified validation workflow, as shown in Fig. 4. In this scheme, band edge positions referenced to NHE at the stated pH define the thermodynamic limits for redox reactions, which must align with the potentials required to generate the observed ROS (*e.g.*, $\cdot O_2^-$, H_2O_2, $\cdot OH$). These reactive species, in turn, must be consistent with the transformation pathways and intermediates identified by chromatography-mass spectrometry analysis. Any mismatch across these levels, such as ROS formation that is not supported by band energetics or intermediates that do not correspond to ROS-driven pathways, indicates mechanistic inconsistency and potential misassignment. This integrated check provides a practical self-consistency criterion that complements multi-technique characterization and helps distinguish physically valid mechanisms from overinterpreted or contradictory claims frequently reported in the literature.

As illustrative cases, we present literature examples that violate thermodynamic–kinetic consistency. As shown in Fig. 5a, Choojun and co-workers assigned the CeO_2/$CoFe_2O_4$ system as a type-I heterojunction photocatalyst, with $\cdot O_2^-$ proposed to form *via* O_2 reduction.[49] However, this contradicts thermodynamic constraints. The $O_2/\cdot O_2^-$ redox potential (−0.046 eV) is more negative than the CBM of $CoFe_2O_4$ (+0.24 eV), indicating electron transfer insufficient to drive O_2 reduction. Thus, considering both thermodynamic feasibility and ROS generation pathways, the type-I heterojunction assignment is incorrect. This is not the case for the polyaniline/β-Bi_2O_3 heterojunction system prepared by Yang and co-workers (Fig. 5b), for example. In their study, the heterojunction was assigned as a type-II system. This assignment is based on the observation that H_2O_2 is generated instead of $\cdot O_2^-$ *via* O_2 reduction by CB electrons in the β-Bi_2O_3 component of the heterojunction. Taking the CBM of β-Bi_2O_3 (+0.23 eV) into account, the corresponding CB electrons should be thermodynamically capable of driving the O_2-to-H_2O_2 transformation, which has a reduction potential of approximately +0.69 V.[50] Thus, the proposed type-II configuration seems correct. Similarly, Jia and co-workers considered thermodynamic–kinetic consistency to assign the heterojunction type in the α-MnO_2/BiOI system (Fig. 6).[51] Two

Table 8 Integrated framework for rigorous evaluation of heterojunction photocatalysts

Category	Key question	Common pitfall	Minimum requirement	Recommended best practice
Mechanism identification	• Is the charge-transfer pathway correctly assigned?	• Band alignment alone used to claim type-II	• Combine XPS/UPS + KPFM/SPV	• Add TAS/TRPL + photodeposition + isotopic tracing
Reactive species validation	• Are the active species correctly identified?	• Assuming mechanism from activity trends	• EPR ($\cdot O_2^-$, $\cdot OH$)	• Correlate with reaction selectivity
Evidence strength	• Is the mechanism supported by robust data?	• Overreliance on PL, EIS, photocurrent	• Use direct techniques (EPR, UPS/XPS, KPFM)	• Multi-technique convergence
Performance interpretation	• Are activity comparisons valid?	• Cross-study ranking without normalization	• Report consistent units and conditions	• Focus on qualitative trends only
Mineralization *vs.* removal	• Is degradation complete?	• Dye decolorization treated as degradation	• TOC/COD analysis	• LC-MS/GC-MS + toxicity evaluation
Photocatalysis artifacts	• Is activity free from experimental bias?	• Dye sensitization, photothermal effects ignored	• Dark/light controls + pH monitoring	• Wavelength-dependent + temperature tracking
Adsorption effects	• Is adsorption separated from reaction?	• Adsorption counted as activity	• Adsorption–desorption equilibrium test	• Kinetic separation modeling
Charge dynamics	• Are carrier behaviors understood?	• Inferring mechanism from PL only	• TRPL or TAS	• Combine with spatial mapping
Stability	• Is the catalyst durable?	• Single-cycle performance reported	• Cycling tests	• Long-term continuous operation
Leaching/integrity	• Is the catalyst stable chemically?	• Ignoring ion release	• ICP analysis	• Operando monitoring
Post-reaction structure	• Does the material remain unchanged?	• No post-analysis	• XRD/XPS after reaction	• *In situ*/operando characterization
Environmental safety	• Are byproducts safe?	• Parent compound disappearance assumed sufficient	• Product identification	• Ecotoxicity assessment
Reproducibility	• Can results be compared?	• Missing experimental details	• Report light source, irradiance, reactor, loading (catalyst, reactant, sacrificial reagent)	• Standardized protocols

possible configurations were considered: a Z-scheme and a type-II heterojunction. ESR analysis confirmed the presence of $\cdot O_2^-$ in the reaction system. If a type-II configuration were assumed, electrons from the CB of BiOI would transfer to the CB of MnO_2. However, the CBM of MnO_2 (+1 eV) is less negative than the reduction potential of $O_2/\cdot O_2^-$ (−0.33 eV), rendering it thermodynamically incapable of driving this reaction. In contrast, under a Z-scheme configuration, the electrons responsible for reducing O_2 to $\cdot O_2^-$ originate from the BiOI component, which has a CBM of approximately +0.5 eV. This is thermodynamically sufficient to drive the oxygen reduction reaction. Therefore, the direct Z-scheme appears to be the correct configuration. However, these interpretations should be treated with caution, as band alignment was assessed for isolated materials rather than for the contacted system. In reality, the interfacial energetics that develop upon semiconductor contact govern the actual charge-transfer pathway. Moreover, in these studies, band positions are assumed to be static, which is insufficient, as charge-carrier accumulation and defect-mediated processes can significantly alter interfacial energetics under operando conditions.

Thus far, heterojunction photocatalysts have been most commonly evaluated for pollutant decomposition, particularly dye decolorization. Therefore, we need to clearly distinguish between apparent pollutant removal and true mineralization in photocatalytic systems for this target reaction. Dye decolorization, reflected as a reduction in UV–vis absorbance, may result from adsorption or partial degradation rather than complete mineralization. Accordingly, a rigorous evaluation of photocatalytic performance should, at a minimum, include TOC or COD analyses to quantify mineralization, complemented by the identification of reaction intermediates and products (*e.g.*, *via* LC-MS or GC-MS) to elucidate degradation pathways and avoid misinterpretation of activity. Failure to implement these criteria may result in overestimation of photocatalytic efficiency and incorrect interpretation of reaction mechanisms.

Equally crucial is the careful consideration of common photocatalytic artifacts to ensure the reliable assessment of both activity and mechanism. Phenomena such as dye sensitization, inner filter effects, photothermal heating, and pH drift can significantly bias experimental outcomes if not properly controlled. Hence, baseline controls, including adsorption–desorption equilibration, light-only and catalyst-only experiments, and continuous pH monitoring, should be considered mandatory. Best practices such as the use of non-sensitizing probe molecules (*e.g.*, phenol, 4-chlorophenol, formic acid, and acetaldehyde), optical filtering or sample dilution to minimize inner filter effects, temperature monitoring to decouple photothermal contributions, and wavelength-dependent studies are strongly recommended.

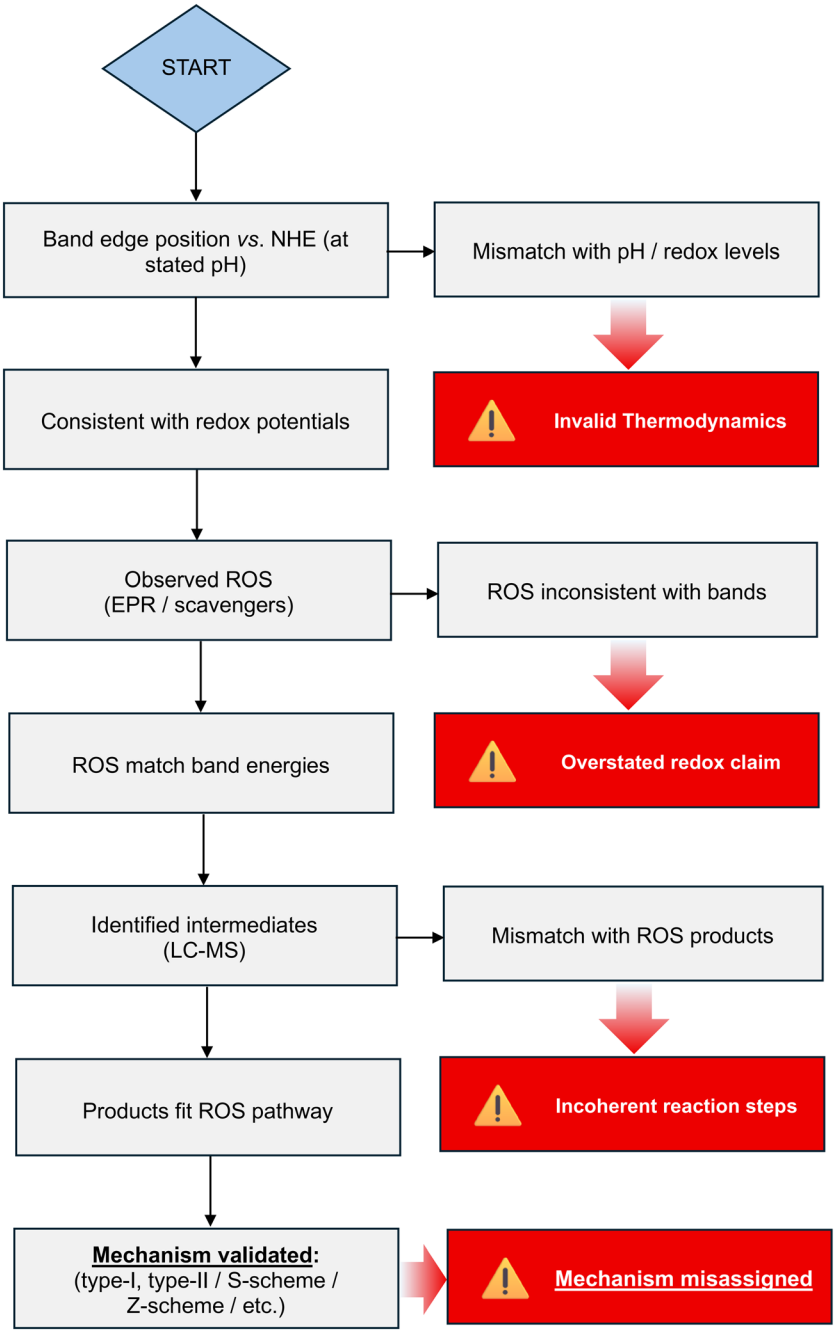

Fig. 4 Thermodynamic–kinetic consistency scheme for validating heterojunction photocatalyst mechanisms.

Overlooking these factors may lead to an overestimation of photocatalytic performance and misinterpretation of charge-transfer mechanisms, as highlighted in Table 2.

Furthermore, when evaluating heterojunction photocatalysts, it is essential to ensure that "safer-by-design" claims are supported by empirical evidence rather than inference. Safer-by-design refers to the deliberate development of materials and processes that minimize environmental and human health risks throughout their lifecycle.[52–54] In this context, a standardized workflow for non-targeted transformation product analysis is critical. Thus, high-resolution mass spectrometry (LC-HRMS), for example, should be employed in full-scan mode, coupled with either data-dependent or data-independent MS/MS acquisition, to enable comprehensive detection of transformation products.[55,56] Rigorous QA/QC procedures, including the use of blanks, replicates, internal standards, and proper instrument calibration, are necessary to ensure data reliability. Compound annotation should follow confidence-based criteria, progressing from exact mass matching to fragmentation analysis and, where possible, confirmation with reference standards. Importantly, the

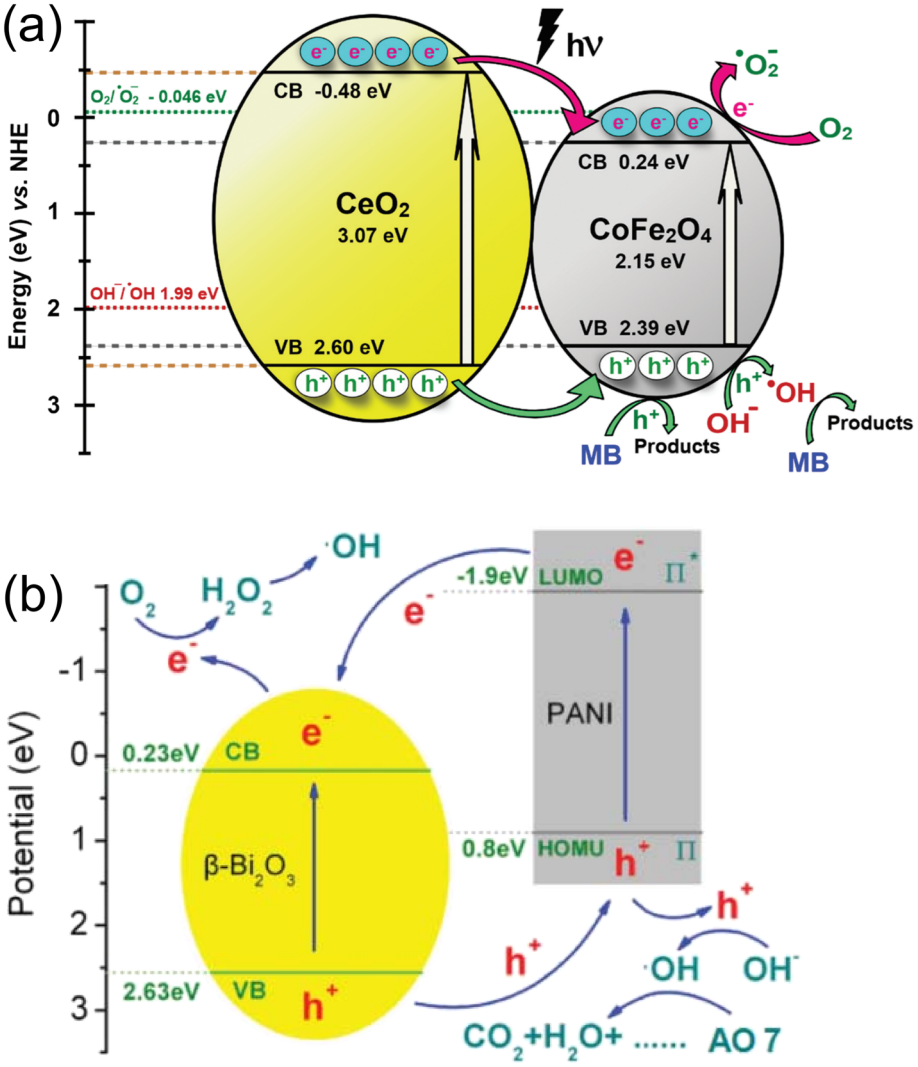

Fig. 5 (a) Schematic illustration of the heterojunction configuration in the $CeO_2/CoFe_2O_4$ system. Reprinted with permission.[49] Copyright 2024, Taylor & Francis. The proposed configuration in the polyaniline/β-Bi_2O_3 heterojunction is shown in panel (b). Reprinted with permission.[50] Copyright 2017, Taylor and Francis.

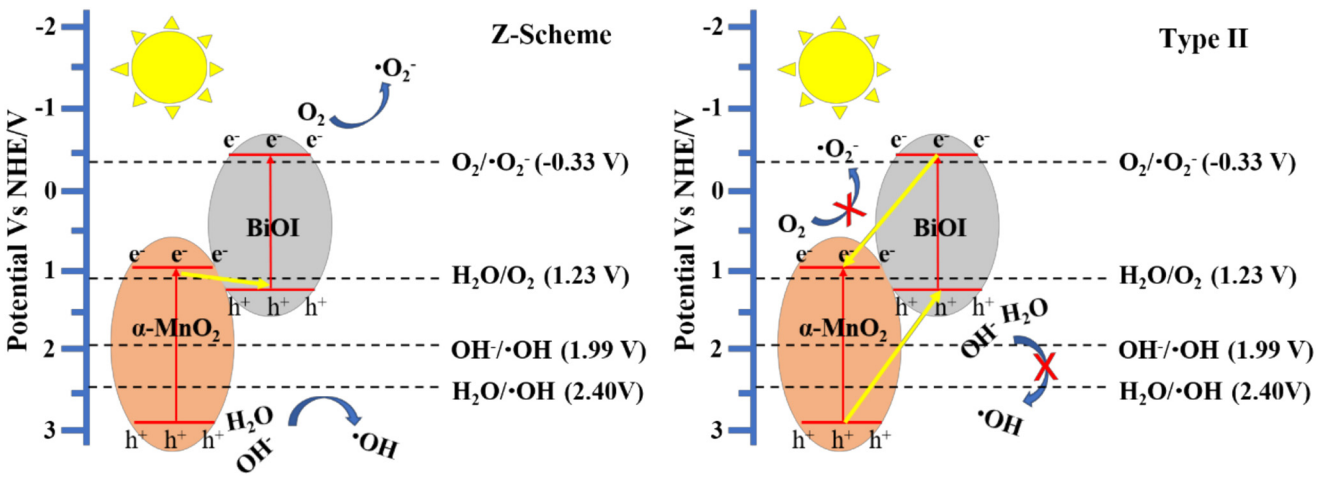

Fig. 6 Schematic illustration of the proposed Z-scheme and type-II charge transfer mechanisms in the α-MnO_2/BiOI heterojunction photocatalyst. Reprinted with permission.[51] Copyright 2022, MDPI.

Table 9 Standardized workflow for non-targeted transformation product analysis

Step	Component	Recommended approach	Purpose
1. Sample preparation	• Quenching & extraction	• Rapid quenching, solid-phase extraction (SPE)	• Preserve intermediates
2. Data acquisition	• LC-HRMS	• Full-scan MS + DDA/DIA MS/MS	• Detect unknown products
3. QA/QC	• Data quality control	• Blanks, replicates, internal standards	• Ensure reliability
4. Feature detection	• Peak picking & alignment	• Software-based (*e.g.*, MZmine, XCMS)	• Identify candidate features
5. Annotation	• Compound identification	• Exact mass + MS/MS fragmentation + databases	• Assign structures
6. Confidence levels	• Identification certainty	• Level 1–5 (confirmed → exact mass only)	• Standardize reporting
7. Quantification	• Semi-quantitative analysis	• Internal standards, relative intensity	• Track product evolution
8. Toxicity linkage	• Effect-directed analysis	• Bioassays (*e.g.*, cytotoxicity, ecotoxicity)	• Link chemistry to effect
9. Data interpretation	• Pathway reconstruction	• Combine kinetics + structure	• Elucidate mechanisms

Note: confidence levels for compound identification should follow widely accepted frameworks (*e.g.*, confirmed structure with reference standard to tentative assignment based on exact mass), and toxicity assessment should be integrated wherever possible to support environmentally relevant conclusions. DDA and DIA refer to data-dependent and data-independent acquisition, respectively, in MS techniques.

Table 10 Environmental validation module for photocatalytic systems from apparent removal to safer-by-design verification

Category	Key question	Minimum requirement	Recommended best practice	Risk if neglected
Apparent removal *vs.* mineralization	• Is pollutant fully degraded?	• TOC or COD analysis	• Carbon mass balance	• False claim of degradation
Parent compound tracking	• Is disappearance correctly interpreted?	• Concentration monitoring (*e.g.*, HPLC/UV-vis)	• Kinetic modeling	• Misleading activity evaluation
Transformation products	• Are intermediates identified?	• LC-HRMS (full scan + MS/MS)	• Time-resolved profiling	• Hidden toxic intermediates
QA/QC (analytical reliability)	• Are data robust?	• Blanks, replicates, calibration	• Isotope-labeled standards	• False positives/negatives
Annotation confidence	• How certain are identifications?	• Exact mass + MS/MS matching	• Reference standard confirmation	• Misassigned structures
Toxicity linkage	• Are products safe?	• Basic toxicity screening	• Effect-directed analysis (EDA)	• "Safer-by-design" unsupported
Photocatalysis artifacts	• Is activity truly photocatalytic?	• Dark/light controls + adsorption test	• Wavelength-dependent + thermal control	• False activity attribution
Catalyst stability	• Is catalyst durable?	• Cycling tests	• Long-term continuous testing	• Unrealistic performance claims
Leaching/ion release	• Is there secondary contamination?	• ICP analysis	• Time-resolved leaching study	• Environmental risk ignored
Post-reaction integrity	• Does catalyst remain unchanged?	• XRD/XPS after reaction	• Operando/*in situ* studies	• Hidden degradation pathways
Byproduct evolution	• Do intermediates accumulate?	• Semi-quantitative tracking	• Reaction pathway reconstruction	• Incomplete mechanism
Environmental relevance	• Are conditions realistic?	• Controlled lab conditions	• Real water matrices testing	• Poor translation to practice

identification of transformation products should be complemented by effect-directed analysis or toxicity assays to establish clear links between chemical structure and biological impact. Such an integrated approach enables a more robust and transparent evaluation of environmental safety in photocatalytic systems. As summarized in Table 9, we propose a standardized workflow for non-targeted transformation product analysis.

Another key consideration is ensuring that photocatalytic performance leads to meaningful environmental benefits. To this end, we propose an integrated environmental validation module (Table 10) that links mineralization, transformation product analysis, toxicity assessment, and catalyst stability. This module establishes minimum requirements for environmental safety validation. Therefore, claims of pollutant removal or safer-by-design performance should only be made when these factors are evaluated in an integrated manner.

5. Practical design

After all, the ultimate issue lies in translating the high performance of laboratory-scale heterojunction photocatalysts into industrial applications, such as large-scale solar water treatment. Photocatalysts intended for practical implementation require more than just enhanced charge separation or broadened light absorption. Industrial systems operate continuously, often outdoors, and under mechanical, chemical, thermal, and hydrodynamic stresses that far exceed controlled laboratory conditions. For example, in a typical laboratory experiment on photocatalytic organic transformations,[57,58] highly selective product formation with complete reactant conversion is often achieved in a reaction volume of less than 10 mL under high-intensity light irradiation often exceeding 1000 W m^{-2}. Such conditions, however, are impractical to reproduce in

real settings. Catalyst design should be informed by realistic operational environments and by how materials evolve under sustained reaction conditions. A heterojunction that performs exceptionally over a few hours in the laboratory may appear promising, but true practical viability demands thousands of hours of stable turnover without loss of structure or activity.

One of the defining characteristics of practical photocatalytic reactors is continuous-flow operation, where reactants rapidly pass over catalyst surfaces. In slurry systems, such hydrodynamic motion generates shear forces that can detach weakly bound nanoparticles, resulting in catalyst loss, environmental contamination, and declining activity. Powder-based heterojunctions are also prone to aggregation under mixing, which reduces their accessible surface area and alters light-harvesting behavior. Immobilizing the photocatalyst on macroscopic supports mitigates these issues by preventing particle loss and ensuring structural stability. However, it often comes at the expense of photocatalytic performance due to decreased illuminated surface area and more limited access to active sites.

Another concern is fouling, which arises from organic impurities, mineral deposits, microbial growth, or by-products of the catalytic reaction itself. Fouling rapidly reduces the active surface area and impairs mass transport. Hierarchical catalysts with open, interconnected pores resist fouling by allowing shear flow to remove impurities and by minimizing dead zones where contaminants accumulate. Conversely, densely packed nanoparticle layers become clogged and irreversibly deactivated.

Chemical robustness is equally crucial. Industrial waters often contain chloride, carbonate, bicarbonate, sulfate, and other ions that can deactivate semiconductor surfaces. Sulfides can oxidize or dissolve; nitrides can hydrolyze; and even carbons can undergo oxidative corrosion under aggressive oxygen-evolution conditions. Thus, the operating environment dictates which semiconductor combinations can realistically survive. Heterojunction systems built from stable oxides and nitrides demonstrate superior resilience, whereas systems relying on more reactive materials must incorporate protective layers.

Beyond mechanical robustness and fouling resistance, practical photocatalytic systems require materials and architectures that preserve redox integrity across broad operational windows. Many laboratory-scale heterojunctions operate efficiently only within narrow pH ranges, often relying on sacrificial agents or highly purified water. Industrial systems, in contrast, must sustain photocatalysis in water containing bicarbonate buffers, hardness ions, and diverse organic impurities, particularly in applications involving treatment of industrial water streams. Such species can quench reactive intermediates or strongly adsorb onto active sites, altering local pH and inhibiting interfacial charge transfer. The ideal heterojunction must therefore retain stable redox potentials and effective charge separation even as surface equilibria dynamically evolve under continuous-flow operation.

Finally, we arrive at the fundamental practical question: which heterojunction configuration and platform are best suited for real-setting applications? Although debate persists within the catalysis community regarding the optimal design, we argue that hierarchical heterojunctions based on S-scheme configurations and integrated with conductive backbones represent the most promising approach. Hierarchical architectures embed nanoscale heterojunctions within macroscale conductive scaffolds such as carbon foams, metal foams, porous ceramics, or structured meshes to harness performance benefits across multiple length scales. At the nanoscale, S-scheme interfaces promote efficient charge separation and strong redox capability. At the mesoscale, the conductive scaffold enables rapid electron extraction, mechanical robustness, and efficient mass transport of reactants and products. At the macroscale, the resulting monoliths can be readily incorporated into flow reactors, flat-plate modules, or monolithic photoelectrochemical panels.

6. Summary

The continued advance of heterojunction photocatalysis depends on replacing convenient but incomplete diagnostics with convergent, mechanism-focused evaluation. The functional behavior of a heterojunction photocatalyst is set by its post-contact energy landscape, shaped by electron redistribution, dipoles, defects, and band bending, not by the flat-band positions of isolated components. Consequently, single-technique inferences (PL quenching, Mott–Schottky shifts, or higher photocurrent) are insufficient for mechanistic claims and often lead to misclassification of type-II, Z-scheme, and S-scheme behaviors. Robust mechanistic assignment requires an integrated toolkit: core-level XPS/UPS shifts to reveal Fermi-level equilibration, KPFM/SPV mapping and Kelvin-probe measurements to visualize built-in fields, TAS/TRPL to resolve carrier populations and lifetimes, EPR to fingerprint oxidative/reductive radicals, and targeted photodeposition or isotopic tracing to localize reactive sites. Material selection must likewise be guided by redox requirements of the target reaction, photochemical stability, interfacial compatibility, carrier mobility, and abundance. For practical deployment, hierarchical S-scheme architectures embedded in conductive, mechanically robust scaffolds combine preserved redox power with scalability, fouling resistance, and enhanced charge extraction. Adopting standardized reporting, operando characterization, and earth-abundant design principles will reduce conceptual confusion, improve reproducibility, and accelerate translation from laboratory demonstrations to durable, real-setting photocatalytic technologies.

Conflicts of interest

The authors declare no conflict of interest.

Data availability

No primary research results, software or code have been included and no new data were generated or analyzed as part of this review.

Acknowledgements

The authors gratefully acknowledge financial support from the National Research and Innovation Agency (Grant No. 3/III.10.4/HK/2023).

References

1 H. Yang, *Mater. Res. Bull.*, 2021, **142**, 111406.
2 F. Li, G. Zhu, J. Jiang, L. Yang, F. Deng and X. Li, *J. Mater. Sci. Technol.*, 2024, **177**, 142–180.
3 H. Sudrajat, Y. Zhou, T. Sasaki, N. Ichikuni and H. Onishi, *Phys. Chem. Chem. Phys.*, 2019, **21**, 5148–5157.
4 Q. Raza, S. Iqbal, T. N. Tamin, A. Fareed, W. A. Al-onazi, M. S. Elshikh, R. Iqbal and M. Jamshaid, *J. Sol-Gel Sci. Technol.*, 2025, **113**, 534–547.
5 Q. Raza, S. Iqbal, F. Bibi, E. Aldosari, A. Kalsoom, M. Jamshaid, R. Iqbal and S. Lim, *J. Sol-Gel Sci. Technol.*, 2025, **114**, 532–548.
6 H. Sudrajat, *Mater. Res. Express*, 2018, **5**, 065519.
7 H. Sudrajat, *Mater. Res. Express*, 2018, **5**, 095501.
8 Q. Raza, G. Fatima, B. Lu, I. Bibi, J. An and S. Lim, *Surf. Interfaces*, 2025, 107203.
9 H. Sudrajat and M. Nobatova, *RSC Appl. Interfaces*, 2025, **2**, 599–619.
10 H. Sudrajat, I. Carra, I. Rossetti, R. Schneider and J. C. Colmenares, *J. Phys. Chem. C*, 2023, **127**, 21881–21914.
11 J. Low, J. Yu, M. Jaroniec, S. Wageh and A. A. Al-Ghamdi, *Adv. Mater.*, 2017, **29**, 1601694.
12 B. Zhu, J. Sun, Y. Zhao, L. Zhang and J. Yu, *Adv. Mater.*, 2024, **36**, 2310600.
13 A. Ganai, P. S. Maiti, L. Houben, R. Bar-Ziv and M. Bar Sadan, *J. Phys. Chem. C*, 2017, **121**, 7062–7068.
14 M. Lin, H. Chen, Z. Zhang and X. Wang, *Phys. Chem. Chem. Phys.*, 2023, **25**, 4388–4407.
15 Q. Su, Y. Li, R. Hu, F. Song, S. Liu, C. Guo, S. Zhu, W. Liu and J. Pan, *Adv. Sustainable Syst.*, 2020, **4**, 2000130.
16 S. J. Moniz, S. A. Shevlin, D. J. Martin, Z.-X. Guo and J. Tang, *Energy Environ. Sci.*, 2015, **8**, 731–759.
17 Z. Han, Y. Song, Y. Jia, Y. Wang, J. Shi, X. Liu, L. Yu, Z. Li, Y. Cheng and H. Zhang, *Adv. Mater. Interfaces*, 2025, **12**, 2500191.
18 X. Wu, M. Sayed, G. Wang, W. Yu and B. Zhu, *Adv. Mater.*, 2026, **38**, e11322.
19 M. Bilal, M. Q. Alfaifi, S. B. Ahmed, M. M. Abduljawad, Y. I. Alrashed, E. S. Aldurahim and Y. A. Alassmy, *Mater. Sci. Semicond. Process.*, 2025, **186**, 109051.
20 T. Li, W. Zhou, Y. Lin, F. Yang, F. Deng and X. Tu, *Curr. Opin. Chem. Eng.*, 2024, **45**, 101042.
21 M. J. Molaei, *J. Am. Ceram. Soc.*, 2024, **107**, 5695–5719.
22 K. Spilarewicz, K. Mróz, M. Kobielusz and W. Macyk, *Curr. Opin. Chem. Eng.*, 2024, **45**, 101041.
23 L. Yuan, P. Du, L. Yin, J. Yao, J. Wang and C. Liu, *Nanoscale*, 2024, **16**, 5487–5503.
24 M. Eshete, X. Li, L. Yang, X. Wang, J. Zhang, L. Xie, L. Deng, G. Zhang and J. Jiang, *Small Sci.*, 2023, **3**, 2200041.
25 N. Chen, D. Luo, P. Chen, S. Li, J. Hu, D. Wang, R. Zhu and Z.-H. Lu, *ACS Energy Lett.*, 2023, **8**, 1313–1321.
26 R. Schlesinger, S. Winkler, M. Brandt, S. Blumstengel, R. Ovsyannikov, A. Vollmer and N. Koch, *Phys. Chem. Chem. Phys.*, 2019, **21**, 15072–15079.
27 G. Shao, *Energy Environ. Mater.*, 2021, **4**, 273–276.
28 P. Zhang, Y. Li, Y. Zhang, R. Hou, X. Zhang, C. Xue, S. Wang, B. Zhu, N. Li and G. Shao, *Small Methods*, 2020, **4**, 2000214.
29 M. J. Shearer, M.-Y. Li, L.-J. Li, S. Jin and R. J. Hamers, *J. Phys. Chem. C*, 2018, **122**, 13564–13571.
30 Z. Meng, J. Zhang, H. Long, H. García, L. Zhang, B. Zhu and J. Yu, *Angew. Chem., Int. Ed.*, 2025, e202505456.
31 C. Cheng, J. Zhang, B. Zhu, G. Liang, L. Zhang and J. Yu, *Angew. Chem., Int. Ed.*, 2023, **62**, e202218688.
32 F. Li, L. Cheng, J. Fan and Q. Xiang, *J. Mater. Chem. A*, 2021, **9**, 23765–23782.
33 J. Yan and J. Zhang, *J. Mater. Sci. Technol.*, 2024, **193**, 18–21.
34 M. Xu, A. Zada, R. Yan, H. Li, N. Sun and Y. Qu, *Phys. Chem. Chem. Phys.*, 2020, **22**, 4526–4532.
35 J. E. Whitten, *Appl. Surf. Sci. Adv.*, 2023, **13**, 100384.
36 H. Cai, B. Wang, L. Xiong, J. Bi, L. Yuan, G. Yang and S. Yang, *Appl. Catal., B*, 2019, **256**, 117853.
37 Y. Wang, Q. Wang, X. Zhan, F. Wang, M. Safdar and J. He, *Nanoscale*, 2013, **5**, 8326–8339.
38 H. J. El-Khozondar, N. Seriani, T. He and F. Xie, *J. Phys. Chem. C*, 2025, **129**, 14593–14597.
39 A. Shabbir, S. Sardar and A. Mumtaz, *J. Alloys Compd.*, 2024, **1003**, 175683.
40 M. Liu, J. Wen, Y. Qin, J. Li, Y. Tang, L. Jiao, Y. Wu, Q. Fang, L. Zheng, X. Cui, W. Gu, C. Zhu, L. Hu and S. Guo, *Sci. China: Chem.*, 2023, **66**, 1228–1236.
41 X. Meng, S. Wang, C. Zhang, C. Dong, R. Li, B. Li, Q. Wang and Y. Ding, *ACS Catal.*, 2022, **12**, 10115–10126.
42 R. Sun, Z. Zhu, N. Tian, Y. Zhang and H. Huang, *Angew. Chem., Int. Ed.*, 2024, **63**, e202408862.
43 X. Xu, S. Dong, J. Lv, G. Huang, Q. Chen and J. Bi, *Appl. Surf. Sci.*, 2025, **689**, 162489.
44 M. Yu, J. Wang, G. Li, S. Zhang and Q. Zhong, *J. Mater. Sci. Technol.*, 2023, **154**, 129–139.
45 Y. Xia, B. Zhu, X. Qin, W. Ho and J. Yu, *Chem. Eng. J.*, 2023, **467**, 143528.
46 L. Xiong and J. Tang, *Adv. Energy Mater.*, 2021, **11**, 2003216.
47 R. Yang, Y. Fan, Y. Zhang, L. Mei, R. Zhu, J. Qin, J. Hu, Z. Chen, Y. Hau Ng and D. Voiry, *Angew. Chem.*, 2023, **135**, e202218016.

48 A. Ganesan, S. Alhowity, A. Z. Alsaleh, M. Guragain, O. Omolere, T. R. Cundari, J. Kelber and F. D'Souza, *J. Electrochem. Soc.*, 2023, **170**, 056501.
49 P. Seeharaj, P. Pasupong and K. Choojun, *J. Asian Ceram. Soc.*, 2024, **12**, 44–58.
50 J. Dai, X. Chen and H. Yang, *Inorg. Nano-Met. Chem.*, 2017, **47**(9), 1364–1368.
51 L. Jia, F. Li, C. Yang, X. Yang, B. Kou, Y. Xing, J. Peng, G. Ni, Z. Cao and S. Zhang, *Catalysts*, 2022, **12**, 1596.
52 E. Söderberg, K. von Borries, U. Norinder, M. Petchey, G. Ranjani, S. Chavan, H. Holmquist, M. Johansson, I. Cotgreave and M. A. Hayes, *Green Chem.*, 2024, **26**, 11147–11163.
53 P. van Gelder, P. Klaassen, B. Taebi, B. Walhout, R. van Ommen, I. van de Poel, Z. Robaey, L. Asveld, R. Balkenende and F. Hollmann, *Int. J. Environ. Res. Public Health*, 2021, **18**, 6329.
54 S. Lin, T. Yu, Z. Yu, X. Hu and D. Yin, *Adv. Mater.*, 2018, **30**, 1705691.
55 J. Aceña, S. Stampachiacchiere, S. Pérez and D. Barceló, *Anal. Bioanal. Chem.*, 2015, **407**, 6289–6299.
56 P. J. Heinsvig, C. Noble, P. W. Dalsgaard and M. Mardal, *TrAC, Trends Anal. Chem.*, 2023, **162**, 117023.
57 S. Reischauer and B. Pieber, *iScience*, 2021, **24**(3), 102209.
58 S. Gisbertz and B. Pieber, *ChemPhotoChem*, 2020, **4**, 456–475.